



This discussion paper is/has been under review for the journal Atmospheric Chemistry and Physics (ACP). Please refer to the corresponding final paper in ACP if available.

# Estimation of mineral dust longwave radiative forcing: sensitivity study to particle properties and application to real cases over Barcelona

M. Sicard<sup>1,2,\*</sup>, S. Bertolín<sup>1</sup>, M. Mallet<sup>3</sup>, P. Dubuisson<sup>4</sup>, and A. Comerón<sup>1</sup>

<sup>1</sup>IRSLab, Universitat Politècnica de Catalunya, Barcelona, Spain

<sup>2</sup>IEEC-CRAE, Universitat Politècnica de Catalunya, Barcelona, Spain

<sup>3</sup>Laboratoire d'Aérodologie, Université de Toulouse/CNRS, Toulouse, France

<sup>4</sup>Laboratoire d'Optique Atmosphérique, Université Lille 1, Villeneuve d'Ascq, France

\* on leave at: Laboratoire d'Aérodologie, Université de Toulouse/CNRS, Toulouse, France

Received: 31 January 2014 – Accepted: 19 March 2014 – Published: 31 March 2014

Correspondence to: M. Sicard (msicard@tsc.upc.edu)

Published by Copernicus Publications on behalf of the European Geosciences Union.

## Estimation of mineral dust LW RF

M. Sicard et al.

Title Page

Abstract

Introduction

Conclusions

References

Tables

Figures

◀

▶

◀

▶

Back

Close

Full Screen / Esc

Printer-friendly Version

Interactive Discussion



## Abstract

The aerosol radiative effect in the longwave (LW) spectral range is sometimes not taken into account in atmospheric aerosol forcing studies at local scale because the LW aerosol effect is assumed to be negligible. At regional and global scale this effect is partially taken into account: aerosol absorption is taken into account but scattering is still neglected. However, aerosols with strong absorbing and scattering properties in the LW region, like mineral dust, can have a non-negligible radiative effect in the LW spectral range (both at surface and top of the atmosphere) which can counteract their cooling effect occurring in the shortwave spectral range. The first objective of this research is to perform a sensitivity study of mineral dust LW radiative forcing (RF) as a function of dust microphysical and optical properties using an accurate radiative transfer model which can compute vertically-resolved shortwave and longwave aerosol RF. Radiative forcing simulations in the LW range have shown an important sensitivity to the following parameters: aerosol load, radius of the coarse mode, refractive index, aerosol vertical distribution, surface temperature and surface albedo. The scattering effect has been estimated to contribute to the LW RF up to 18 % at the surface and up to 38 % at the top of the atmosphere. The second objective is the estimation of the shortwave and longwave dust RF for 11 dust outbreaks observed in Barcelona. At the surface, the LW RF varies between +2.8 and +10.2 W m<sup>-2</sup>, which represents between 11 and 26 % (with opposite sign) of the SW component, while at the top of the atmosphere the LW RF varies between +0.6 and +5.8 W m<sup>-2</sup>, which represents between 6 and 26 % (with opposite sign) of the SW component.

## 1 Introduction

Atmospheric aerosols have a remarkable effect on the Earth–atmosphere radiative budget (Foster et al., 2007). Indeed, aerosols and their interactions with clouds contribute to the largest uncertainties in the estimation of the Earth’s changing energy

ACPD

14, 8533–8573, 2014

## Estimation of mineral dust LW RF

M. Sicard et al.

Title Page

Abstract

Introduction

Conclusions

References

Tables

Figures

◀

▶

◀

▶

Back

Close

Full Screen / Esc

Printer-friendly Version

Interactive Discussion



**Estimation of mineral dust LW RF**

M. Sicard et al.

Title Page

Abstract

Introduction

Conclusions

References

Tables

Figures

◀

▶

◀

▶

Back

Close

Full Screen / Esc

Printer-friendly Version

Interactive Discussion



budget (IPCC, 2013). Nowadays many radiative transfer models (RTM) have been developed to locally estimate the aerosol direct radiative forcing (RF) (Ricchiazzi et al., 1998; Key et al., 1998; Mayer et al., 2005; Berk et al., 2006). Some recent studies focused only in the estimation of the shortwave (SW) RF arguing that the contribution of the longwave (LW) component was negligible (Roger et al., 2006; Mallet et al., 2008; Sicard et al., 2012). Few studies have considered the LW range due to the difficulties to parameterize accurately the model and the lack of knowledge of the aerosol properties in the LW range. A selection of reference papers including the longwave radiative impact is: Fouquart et al. (1987), Sokolik and Golitsyn (1993), Sokolik et al. (1993, 1998), Liao and Seinfeld (1998), Dufresne et al. (2002), Markowicz et al. (2003) and Vogelmann et al. (2003).

It is true that the RF of most aerosol types (especially for fine particles such as pollution and smoke) in the LW range is small compared to their forcing in the shortwave. However large, highly absorbing and scattering particles such as mineral dust (MD) have revealed to have a significant forcing in the LW (Fouquart et al., 1987; Dufresne et al., 2002). Mineral dust is an atmospheric aerosol present all around the world, even though it is originated only in a few delimited sources. In Europe the nearest source is the Sahara desert, which is the largest one, emitting half of the world atmospheric MD (Prospero et al., 2002). During its transport, MD properties are modified in such a manner that only a medium-size distribution remains (very small and very large particles are deposited through wet scavenging and sedimentation mechanisms, respectively) (Osada et al., 2014). In addition to dust particles, sea salt is also a type of particle that could potentially have a significant forcing in the LW range for its large size and absorbing properties in the LW region (Li et al., 2008). However, sea salt particles are usually confined to the bottom of the planetary boundary layer, which prevents them from having an impact on radiance collected at the top of the atmosphere. The radiative impact of sea salt alone is difficult to evaluate in urban areas as Barcelona where it is mixed with local, urban aerosols. For those reasons sea salt is discarded from our

study which concentrates on mineral dust particles only. To characterize the properties of the “typical” MD transported to our region, a climatology development is proposed.

In this study we start with a rather complete review of the existing knowledge of the MD microphysical and optical properties in the LW spectral range and establish a climatology characterizing the properties of the “typical” transported MD observed in our region. We examine first the sensitivity of LW RF to aerosol properties (particle size, fine/coarse mode ratio) and aerosol layer properties (aerosol optical thickness, layer height) and then the LW scattering effect. The latter process is generally neglected in regional and global climate models (Yoshioka et al., 2007; Lau et al., 2009; Zhao et al., 2011). This sensitivity study is conducted using the state-of-the-art radiative transfer model GAME (Dubuisson et al., 1996). Also, we identify real situations with high dust loads observed in Barcelona and estimate SW and LW clear-sky direct radiative forcings using combined lidar, sun-photometer and satellite observations.

## 2 Mineral dust model in Barcelona

Among the broad literature available on atmospheric aerosol microphysical and optical properties, many works deal with the characterization of MD particles, though in the LW spectral range, the available literature reduces significantly. MD particles are well characterized by remote sensing observations (Kaufman et al., 2002; Dubovik et al., 2002; Remer et al., 2008; Tanré et al., 2011) and laboratory experiments (Volz, 1972, 1973, 1983), or a combination of both (d’Almeida et al., 1991; Krekov, 1993; Hess et al., 1998). In order to find a model of MD particles representative of long-range transported particles over Barcelona, a climatology of sun-photometer-derived products is established. Some parameters such as the particle shape, the refractive index, the particle density and the vertical distribution are defined through references.

Yang et al. (2007) showed that “the nonsphericity effect of dust particles is significant at short wavelengths but not at the thermal infrared wavelengths.” For this reason parti-

### Estimation of mineral dust LW RF

M. Sicard et al.

Title Page

Abstract

Introduction

Conclusions

References

Tables

Figures

◀

▶

◀

▶

Back

Close

Full Screen / Esc

Printer-friendly Version

Interactive Discussion



cles are assumed to be spherical and the classical Mie theory is employed to compute their optical properties used as input in the GAME RTM.

## 2.1 Refractive index

Contrary to the shortwave range, small spectral variations in the refractive index in the LW can result in significant changes in the optical coefficients such as the extinction coefficient or the single scattering albedo. Hence, a good spectral resolution is needed.

The behavior of the real and the imaginary part of the refractive index of MD particles as a function of wavelength in the LW has been reported for the first time in a limited number of studies performed more than two decades ago (Volz, 1972, 1973, 1983; Fouquart et al., 1987). The refractive index of MD particles as a function of wavelength in the LW has also been treated later in reference books about atmospheric aerosols such as (d'Almeida et al., 1991; Krekov, 1993) and in the software package OPAC (Optical Properties of Aerosols and Clouds) (Hess et al., 1998). There, the authors have compiled previous studies and have come up with “corrected” refractive indices.

The values of the refractive index considered here come from measurements taken in Meppen in western Germany (Volz, 1983). The table giving the refractive index as a function of the wavelength was found in Krekov (1993). MD particles, including soot, one of the main drivers of the absorption, were obtained after removal of water solubles and of particles with radii greater than  $1.5\ \mu\text{m}$  (Volz, 1983). Figure 1 shows the variation of the MD refractive index as a function of wavelength from  $0.2$  to  $40\ \mu\text{m}$ . For comparison indices from Volz (1973) and Hess et al. (1998) are also reported. The figure shows large spectral variations in the infrared atmospheric window ( $8$ – $13\ \mu\text{m}$ ), which have an important impact on the infrared radiative budget of the atmosphere. The real parts of the refractive index,  $n_r$ , are nearly equal in the entire spectral range. The imaginary part,  $n_i$ , of Volz (1983) differs from the two others in two regions. It is lower above  $18\ \mu\text{m}$ . However, this difference in  $n_i$  will have a negligible impact on the radiative forcing calculations as the radiative forcing at wavelengths greater than  $15\ \mu\text{m}$  is close to zero (see Sect. 4). In the  $3$  to  $8\ \mu\text{m}$  range the imaginary part of Volz (1983)

## Estimation of mineral dust LW RF

M. Sicard et al.

Title Page

Abstract

Introduction

Conclusions

References

Tables

Figures

◀

▶

◀

▶

Back

Close

Full Screen / Esc

Printer-friendly Version

Interactive Discussion



## Estimation of mineral dust LW RF

M. Sicard et al.

Title Page

Abstract

Introduction

Conclusions

References

Tables

Figures

◀

▶

◀

▶

Back

Close

Full Screen / Esc

Printer-friendly Version

Interactive Discussion



is clearly above the others, by a value of  $\sim 0.05$ . The most probable reason for that difference is the MD origin: Volz (1973) and Hess et al. (1998) do not refer directly to transported mineral dust. For example, the refractive index in Hess et al. (1998) is dominantly from d'Almeida et al. (1991) who defines a dust-like aerosol by measuring soil dust obtained by evaporation of rain and snow water (Volz, 1972), without referring directly to MD. Finally the refractive index of Volz (1983) is also in good agreement with more recent studies such as Otto et al. (2007) who calculated a mean real and imaginary part extracted from a wide range of the literature data by applying a moving average, emphasizing the large variability of the dust refractive index in literature. In a lesser extent the measurements from McConnell et al. (2010) are, on average, also in agreement with the refractive index chosen in this study at least between 6 and  $10\ \mu\text{m}$  (no data are shown above  $10\ \mu\text{m}$  in McConnell et al., 2010).

## 2.2 Size distribution, concentration and AOT

The MD size distribution and concentration have been retrieved by long-term AERONET (Aerosol Robotic Network) (Holben et al., 1998) sun-photometer measurements in Barcelona during the period 23 December 2004–15 September 2012. Only level 2 data have been considered. In the above mentioned period a total of 4529 size distribution inversions are available.

MD particles have been discriminated by applying the method described in Gobbi et al. (2007) and Basart et al. (2009) that classifies the aerosols as MD when the Ångström exponent,  $AE_{440,870}$ , is less than 0.75, and the difference  $\delta AE = AE_{440,675} - AE_{675,870}$  is less than 0.3.  $AE_{\lambda_1, \lambda_2}$  refers to the Ångström exponent calculated between the two wavelengths  $\lambda_1$  and  $\lambda_2$ . To guarantee errors lesser than 30 %, Gobbi et al. (2007) recommend to apply an additional criterion on the aerosol optical thickness (AOT) at 675 nm:  $AOT > 0.15$ . The distribution of all points with  $AOT > 0.15$  at 675 nm is shown in Fig. 2 in a so-called  $\delta AE$  vs.  $AE$  plot. The measurements representatives of MD particles according to the discrimination described above fall inside the red rectangle: there are a total of 134 measurements, distributed over 54 days. The

## Estimation of mineral dust LW RF

M. Sicard et al.

Title Page

Abstract

Introduction

Conclusions

References

Tables

Figures

◀

▶

◀

▶

Back

Close

Full Screen / Esc

Printer-friendly Version

Interactive Discussion



average size distribution of those 134 measurements, represented in Fig. 3, shows the strong predominance of the coarse mode as expected. Incidentally it is very similar in shape and magnitude to the size distribution of a MD event with AOTs at 500 nm of  $\sim 0.38$  and described as typical MD aerosol conditions in southwestern Spain (Cachorro et al., 2008). The mean values of the fine and coarse volume median radii,  $r_{V,f}$  and  $r_{V,c}$ , their associated standard deviations,  $\sigma_{V,f}$  and  $\sigma_{V,c}$ , their volume concentrations,  $C_{V,f}$  and  $C_{V,c}$ , respectively, and the total AOT at 500 nm are reported in Table 1. All those magnitudes are products from the AERONET inversion code (Dubovik and King, 2000; Dubovik et al., 2000). Because of the long-range transport of the MD between the source and the region of Barcelona, the coarse mode radius and volume concentration ratio found here ( $r_{V,c} = 2.001 \mu\text{m}$  and  $C_{V,c}/C_{V,f} \sim 5$ ) are lower than those measured near the MD source in Bahrain, Persian Gulf, ( $r_{V,c} = 2.540 \mu\text{m}$  and  $C_{V,c}/C_{V,f} \sim 10$ ) and in Solar-Village, Saudi Arabia, ( $r_{V,c} = 2.320 \mu\text{m}$  and  $C_{V,c}/C_{V,f} \sim 50$ ) (Dubovik et al., 2002), which are representative of so-called pure desert dust. The mean total AOT at 500 nm is  $0.37 \pm 0.13$ . Because of the influence of MD this value is much larger than the mean summer AOT of 0.20 (at 532 nm) measured in Barcelona (Sicard et al., 2011).

The input of our Mie code is the median (equivalent to the geometric mean) radius,  $r_g$ , and the standard deviation,  $\sigma_g$ , of the lognormal distribution, as well as the particle number,  $N$ . The conversion of AERONET volumetric products to those parameters is given in the Appendix.

### 2.3 Mineral dust model in Barcelona

The climatology established in Sect. 2.2 allows for the determination of the most representative model of MD observed in our region. In order to determine how the MD events are distributed over the year in Barcelona, we represent in Fig. 4 the number of days per month of MD observed by the AERONET sun-photometer. The discrimination method from Gobbi et al. (2007) has been used on all the AOT retrievals from AERONET in the period 23 December 2004–15 September 2012. 270 days were found, which, over the whole period, represents 9.6 % of the time. This value is lower than the 17 % of African







as:

$$\Delta F_{\text{BOA}} = F_{\text{BOA}}^{\text{w}} \downarrow - F_{\text{BOA}}^{\text{o}} \downarrow \quad \text{and} \quad (1)$$

$$\Delta F_{\text{TOA}} = - \left( F_{\text{TOA}}^{\text{w}} \uparrow - F_{\text{TOA}}^{\text{o}} \uparrow \right), \quad (2)$$

where  $F^{\text{w}}$  and  $F^{\text{o}}$  are the radiative fluxes with and without aerosols, respectively. The  $\downarrow$  and  $\uparrow$  arrows indicate if the fluxes are downward or upward, respectively. With this convention, a negative sign of the daily  $\Delta F$  implies an aerosol cooling effect. In this study the SW and LW spectral components have been treated separately. A description of the model in the SW spectral region can be found in Roger et al. (2006), Mallet et al. (2008) and Sicard et al. (2012).

### 3.1 Model description in the LW spectral range

GAME accounts for thermal emission, absorption and scattering, as well as their interactions, using the Discrete Ordinates Method (DISORT) (Stamnes et al., 1988). This accurate method allows calculating solar and thermal infrared fluxes (from 0.2 to 50  $\mu\text{m}$ ) at any atmospheric level with the assumption of a vertically inhomogeneous media, stratified into plane and homogeneous layers. In addition, the GAME code has a fixed spectral resolution ( $\Delta\nu = 20 \text{ cm}^{-1}$ ) over the whole infrared spectral range.

Gaseous absorption ( $\text{H}_2\text{O}$ ,  $\text{CO}_2$ ,  $\text{O}_3$ ,  $\text{N}_2\text{O}$ ,  $\text{CO}$ ,  $\text{CH}_4$  and  $\text{N}_2$ ) is treated from the correlated  $k$ -distribution (Lacis and Oinas, 1991). Considering a layer at pressure  $P$  and temperature  $T$ , the transmission function for a spectral interval  $\Delta\nu$  is approximated by an exponential summation over a limited number  $N$  of absorption classes as:

$$T_{\Delta\nu}(P, T) = \sum_{i=1}^{MN} a_i \exp[-k_i(P, T)u(P, T)], \quad (3)$$

with  $u$  the absorber amount. The weight  $a_i$  represents the probability associated to the mean absorption coefficient  $k_i$  for each absorption class  $i$ . The coefficients of the

## Estimation of mineral dust LW RF

M. Sicard et al.

Title Page

Abstract

Introduction

Conclusions

References

Tables

Figures

◀

▶

◀

▶

Back

Close

Full Screen / Esc

Printer-friendly Version

Interactive Discussion



**Estimation of mineral dust LW RF**

M. Sicard et al.

Title Page

Abstract

Introduction

Conclusions

References

Tables

Figures

◀

▶

◀

▶

Back

Close

Full Screen / Esc

Printer-friendly Version

Interactive Discussion



exponential series ( $a_i$  and  $k_i$ ) have been determined with reference calculations from a Line-By-Line (LBL) code (Dubuisson et al., 1996, 2005), using the spectroscopic database HITRAN (Rothman et al., 2009). The coefficients  $a_i$  and  $k_i$  are then calculated for a set of reference pressure  $P$  and temperature  $T$  with the LBLDOM (LBL Discrete Ordinates Method) code (Dubuisson et al., 1996). For a given atmospheric profile, these coefficients are calculated using interpolations. Note that the correlated  $k$ -distribution technique allows accounting for interaction between gaseous absorption and multiple scattering with manageable computational time. In addition, the impact of the absorption continua is modelled using the CKD (Clough, Kneizys and Davis) formulation (Clough et al., 1989).

One of the main specificity of the GAME code in the LW range is the complete representation of the LW aerosol scattering which is most of time neglected in regional and global climate models in spite of its effect on the LW RF (Yoshioka et al., 2007; Lau et al., 2009; Zhao et al., 2011). Indeed, Dufresne et al. (2002) have shown that the TOA LW RF could be increased by about 50 % when this process is taken into account. The scattering effect is included in the sensitivity study proposed in this work, but the study has been refined compared to Dufresne et al. (2002) to be more representative of long-range transported MD: Dufresne et al. (2002) used an AOT of 1 at 500 nm which is much higher than the mean AOT of 0.37 of our MD model. The spectral optical properties of aerosols are defined for each atmospheric layer, including the moments of the phase function, the single scattering albedo and the extinction optical thickness. The high spectral resolution of GAME allows accounting for the spectral variations of aerosol properties, especially in the infrared window.

### 3.2 Model parametrization

Besides aerosol optical properties, the RTM is sensitive to atmospheric parameters such as the relative humidity and the air temperature profiles, the surface emissivity and temperature or the aerosol vertical distribution. Some other parameters (e.g. the

sun position) are involved in the calculation but are not commented here, because they have a negligible effect on the LW RF.

### 3.2.1 Atmospheric profiles

In a first approximation the RTM model was run with a mid-latitude summer (MLS) profile taken from the US Standard Atmosphere, 1976 model (McClatchey et al., 1972). In order to check how the model compares to real atmospheric profiles, we use the results from Sicard et al. (2013) in which the MLS profiles are compared to the seasonal mean profiles of temperature, pressure and relative humidity measured by radiosoundings launched every day in Barcelona between June 2008 and February 2013 at 12:00 UT.

The mean profiles of the joined spring and summer seasons have also been calculated, as the spring and summer seasons represent together two thirds of the MD frequency in Barcelona (see Sect. 2.3). In general the MLS model overestimates the values of temperature and relative humidity at all heights and for all seasons, while the profiles of pressure are all similar. Similarities were found between the MLS and the summer temperature profiles and between the MLS and the autumn relative humidity profiles. Those similarities have a direct impact on the LW RF also given in Sicard et al. (2013) as a function of wavelength: the MLS and the summer profiles give very similar RF at the BOA, while the best agreement at the TOA is obtained for the autumn season. The largest difference between the MLS and the spring-summer period occurs at the TOA and nearly reaches 30 %. Because the MLS and the spring-summer profiles give quite different RF, the latter are used in the sensitivity study.

### 3.2.2 Surface properties

Contrary to the shortwave region, where the albedo (or reflectivity),  $\rho$ , can be highly directional, in the LW it is possible to approximate the surface as lambertian. If Earth is considered in thermodynamic equilibrium, the emissivity,  $\varepsilon$ , is related to the albedo by  $\varepsilon = 1 - \rho$ . The surface emissivity has been calculated as the mean surface emissivity

## Estimation of mineral dust LW RF

M. Sicard et al.

Title Page

Abstract

Introduction

Conclusions

References

Tables

Figures

◀

▶

◀

▶

Back

Close

Full Screen / Esc

Printer-friendly Version

Interactive Discussion



## Estimation of mineral dust LW RF

M. Sicard et al.

Title Page

Abstract

Introduction

Conclusions

References

Tables

Figures

◀

▶

◀

▶

Back

Close

Full Screen / Esc

Printer-friendly Version

Interactive Discussion



measured by the CERES (Clouds and the Earth's Radiant Energy System) sensor in the spectral range of its WN "window" (8.1 to 11.8  $\mu\text{m}$ ) for the seasons of spring and summer between June 2007 and May 2012. The corresponding surface albedo is 0.017. The associated standard deviation is 0.001 indicating a very low variability of this parameter (its minimum and maximum values are 0.013 and 0.018, respectively).

The average surface temperature measured by CERES for the same seasons of spring and summer is 297.49 K with an associated standard deviation of 6.56 K (minimum and maximum values of 279.64 and 318.52 K, respectively). Those values are summarized in Table 2.

### 3.2.3 Aerosol stratification

The aerosol vertical distribution was set to the MD layer characteristics based on observations over a period of 3 years (Papayannis et al., 2008). In Barcelona, the MD layer base mean is  $1434 \pm 441$  m and the top mean is  $3608 \pm 1605$  m. In order to adjust those layers to the vertical levels defined in GAME, the MD vertical distribution in Barcelona has been set to 1500–3500 m. In those layers the extinction coefficient has a mean value of  $\sim 70 \text{ Mm}^{-1}$  with peaks that can exceed  $100 \text{ Mm}^{-1}$  (Sicard et al., 2011).

## 4 Sensitivity study in the longwave spectral range

The MD model parameters and the generic parameters of the sensitivity study are given in Tables 1 and 2, respectively. Figures 6 and 7 show the LW RF as a function of different parameters. Figure 6 shows the LW spectral RF as a function of wavelength at the BOA and at the TOA, respectively, and for the fine and the coarse mode. Most of the forcing occurs in the atmospheric window of 8 to 13  $\mu\text{m}$  where large spectral variations of the refractive index occur (see Sect. 2.1). The spectral forcing at the surface is about twice higher than at the TOA. This is due to the fact that the main source of LW radiation, the Earth, is close to the surface. At the TOA, the overall effect of aerosols is

to reduce the upward longwave radiation emitted by the surface through absorption and scattering. At the TOA large particles have also a non-negligible effect on the spectral RF in the 17 to 22  $\mu\text{m}$  range. At both the BOA and the TOA the effect of small particles represents approximately 10 % of the LW spectral RF.

5 The LW RF at the BOA and the TOA as a function of AOT at 500 nm is shown in Fig. 7a. As the height of the MD layer (1.5–3.5 km) is relatively close to the surface, the effect of the aerosol emission is here again to make the RF at the BOA higher than at the TOA.

10 Figure 7b shows the behaviour of the RF as a function of the MD layer height, assuming a MD layer thickness of 1 km. Aerosols scatter, absorb and re-emit radiation in all directions. The scattering occurs preferably in the forward direction ( $g \approx 0.5$  in the 8 to 13  $\mu\text{m}$  range, Fig. 5). Earth surface is the principal source of LW radiation so that the closer the aerosol layer from the surface, the more radiation will be reflected. This is well reproduced in Fig. 7b where the LW RF is high near the surface and decrease with increasing height while at the TOA it behaves oppositely.

15 Figure 7c shows the particle size dependency of the LW RF for a constant AOT of 0.37 at 500 nm. The size distribution is assumed monomodal and the AOT is maintained constant by adjusting the particle number,  $N$ . To maintain the AOT constant for small particles, it is necessary to increase the particle number to unrealistically large values. For  $r_g < 0.02 \mu\text{m}$   $N$  has to be larger than  $\sim 1000 \text{cm}^{-3}$ . This value of  $N$  was measured by Wagner et al. (2009) inside a dust plume with an AOT of  $\sim 0.4$  at 440 nm (higher than the AOT of 0.37 at 500 nm of our MD model) for submicronic particles. Thus we set this value of  $N$  as the upper limit beyond which Fig. 7c stops from having a physical meaning. In the figure the region in which  $N$  exceeds that limit, and therefore the curves lose their physical meaning, is marked by a semi-transparent, grey rectangle. It is also worth noting that for small particles the size parameter  $x = \frac{2\pi r_g}{\lambda}$  is smaller than 0.1 in the LW spectral range which is the lower limit of the range defining the “Mie regime”. For those small particles the Mie theory is therefore not adapted to calculate the particle optical properties. For those two reasons the region in grey in Fig. 7c is

---

**Estimation of mineral dust LW RF**M. Sicard et al.

---

[Title Page](#)[Abstract](#)[Introduction](#)[Conclusions](#)[References](#)[Tables](#)[Figures](#)[◀](#)[▶](#)[◀](#)[▶](#)[Back](#)[Close](#)[Full Screen / Esc](#)[Printer-friendly Version](#)[Interactive Discussion](#)

## Estimation of mineral dust LW RF

M. Sicard et al.

Title Page

Abstract

Introduction

Conclusions

References

Tables

Figures

◀

▶

◀

▶

Back

Close

Full Screen / Esc

Printer-friendly Version

Interactive Discussion



not discussed. Between 0.02 and 0.5  $\mu\text{m}$  in radius the absorption coefficient decreases and the single scattering albedo increases from nearly zero. From 0.5  $\mu\text{m}$ , the absorption as well as the scattering increase, hence the increase in the RF seen in Fig. 7c. We note that the LW RF of the MD model (+6.02  $\text{W m}^{-2}$  at the BOA and +3.58  $\text{W m}^{-2}$  at the TOA, see the RF in Fig. 7a at the red arrow) falls between the two red arrows indicating the fine and coarse mode of the MD model.

Figure 7d shows the LW RF as a function of the particle size maintaining constant the volume occupied by the particles. A monomodal distribution is considered. We depart from particles with a median radius  $r'_g = 1 \mu\text{m}$  and calculate the particle number,  $N'$ , necessary to obtain an AOT of 0.37. For all the values of  $r_g$  explored in Fig. 7d the product  $(r_g)^3 \times N$  is maintained constant and equal to  $(r'_g)^3 \times N'$ . Here again, it is necessary to increase the particle number to unrealistically large values to maintain the product  $(r_g)^3 \times N$  constant for small particles: the limit of  $N = 1000 \text{ cm}^{-3}$  is reached for particles with a radius of 0.03  $\mu\text{m}$ . The semi-transparent, grey rectangle in Fig. 7d represents the region where  $N$  exceeds that limit and where the figure is not discussed. We have mathematically checked that maintaining constant the volume occupied by the particles is equivalent to maintaining constant the volume concentration  $C_V$ . For particles with a radius lower than 0.1  $\mu\text{m}$  nearly all the extinction is due to absorption ( $\omega_0 = 0$ ), while for greater radius the optical properties are similar to those of Fig. 5. For very large particles ( $r_g > 10 \mu\text{m}$ ),  $\omega_0 \approx 0.5$  and  $N$  is very low. This produces the LW RF to be nearly 0. In Fig. 7d the LW RF neglecting scattering (grey lines) clearly show that for radii lower than 0.1  $\mu\text{m}$  the scattering properties have no effect on the LW RF. For radii greater than 0.1  $\mu\text{m}$ , the scattering effect contributes to the LW RF up to 18 % at the BOA and up to 38 % at the TOA. The highest contribution is reached for particles with a radius of 0.5  $\mu\text{m}$ , which is close to the coarse radius of our MD model, 0.649  $\mu\text{m}$ . This point emphasizes the importance of the scattering effect when studying the LW RF of long-range transported MD.

Figure 7e shows the LW RF dependency on the ratio of coarse to fine mode particle concentration,  $N_c/N_f$ . One sees that the amount of RF produced by small particles is

less than 14 % at the BOA and less than 10 % at the TOA compared to that produced by large particles. Figure 7e follows the same shape as the single scattering albedo vs.  $N_c/N_f$  at 8.5  $\mu\text{m}$  for “Sahara dust-Barbados” aerosol type shown in Sokolik et al. (1998). According to the results from Sokolik et al. (1998) ( $\omega_0$  vs.  $N_c/N_f$  nearly constant at 11 and 12  $\mu\text{m}$ , and increasing at 8.5  $\mu\text{m}$ ), we conclude that the increase of RF with increasing  $N_c/N_f$  is mostly due to the low values of the single scattering albedo around the wavelength of 8  $\mu\text{m}$  (see Fig. 5).

Finally Fig. 7f and g shows the LW RF as a function of the surface temperature (in the range 0–40 °C) and the surface albedo (in the range 0–0.3), respectively. The range of the surface albedo was chosen according to the results from Wang et al. (2005) in which the spectral emissivity of many kind of ground materials has been estimated and is always larger than 0.7 in the spectral range from 3 to 14  $\mu\text{m}$ . From Fig. 7f the LW RF at the TOA is more sensitive to surface temperature change than the LW RF at the surface. This figure illustrates well the works from Dufresne et al. (2002) in which a simple conceptual model formalizes that sensitivity: the LW RF at the TOA is proportional to the absorption and reflection coefficients of the aerosol layer (that multiplies the upward irradiance at the surface which depends directly on the surface temperature) whereas at the BOA it is proportional to the reflection coefficient. Figure 7g shows that the LW RF decreases with increasing surface albedo. This result was expected since as the surface albedo increases, its emissivity decreases and therefore less LW radiation reaches the aerosol layer.

## 5 Application to real cases over Barcelona

The RF is estimated for 11 real cases of MD outbreaks in Barcelona which took place between 2007 and 2012. All cases are documented by lidar, sun-photometer, radiosoundings and CERES measurements and have been identified as MD outbreaks by applying the method described in Gobbi et al. (2007) (see Sect. 2.2). Both the SW

## Estimation of mineral dust LW RF

M. Sicard et al.

Title Page

Abstract

Introduction

Conclusions

References

Tables

Figures

◀

▶

◀

▶

Back

Close

Full Screen / Esc

Printer-friendly Version

Interactive Discussion





and LW radiative forcings have been calculated with the GAME code. Some details of those 11 cases are listed in Table 3.

In order to check the suitability of GAME to estimate correctly the outgoing LW radiation (OLR) at the TOA, fluxes simulated with GAME are compared to those measured by CERES (Fig. 8) for the 11 cases. At the surface such a comparison is not possible because of the lack of flux measurements in the LW spectral range in Barcelona. CERES measurements are either from the AQUA satellite (overpass over Barcelona between 1200 and 13:00 UT) or from the TERRA satellite (overpass over Barcelona between 1000 and 10:30 UT). The time difference between CERES and the lidar measurements (taken as the instantaneous simulation time in GAME) is not relevant neither in terms of solar LW radiation since the latter is nearly constant during daytime hours, nor in terms of surface albedo since the latter is also quite constant (see Sect. 3.2.2). The only parameter on which the time difference could have an impact is the surface temperature. Another difference is the spectral range: CERES measurements are in the spectral range of its WN “window” defined between 8.1 and 11.8  $\mu\text{m}$  whereas the fluxes calculated by GAME are in the range 8.06–11.9  $\mu\text{m}$ . Figure 8 shows a moderate variability of the points around the 1/1 line which is reflected by a root mean square (RMS) of 2.52  $\text{W m}^{-2}$ . However there are approximately the same number of points above and below the 1/1 line which means that GAME OLR does not present a systematic bias compared to CERES OLR. The normalized bias, equal to  $-0.8\%$ , is very low indeed. We would like to draw the attention to the difficulties of extracting any magnitude from CERES pixels in coastal areas, such as Barcelona. In such areas some pixels are not representative neither of land, nor of sea because they contain information from both sources. For that reason, we have carefully selected CERES pixels to be over land, but to do so we have had to select pixels sometimes as far as  $\sim 40$  km where the soil type is different from that of the city center. The quantitative agreement between the observed and modeled OLR does provide an important check on the accuracy of GAME.

To perform the LW calculations with GAME, the refractive index has been taken as in Table 1. The MD size distribution and concentration were taken from the AERONET

## Estimation of mineral dust LW RF

M. Sicard et al.

Title Page

Abstract

Introduction

Conclusions

References

Tables

Figures

◀

▶

◀

▶

Back

Close

Full Screen / Esc

Printer-friendly Version

Interactive Discussion



sun-photometer level 2.0 inversion products the closest in time to the lidar measurement time. For each case the profiles of pressure, temperature and relative humidity were taken from the radiosoundings at 12:00 UT of the corresponding day. The surface albedo was calculated from the surface emissivity measured by CERES and the surface temperature was taken directly from CERES. The AOT vertical distribution was retrieved by means of lidar-derived extinction profiles at 532 nm.

The SW and LW RF calculated by GAME at the BOA and at the TOA for the 11 cases of MD are given in Table 3 and represented in Fig. 9a and b. The RF of the aerosols in the whole atmospheric column is represented in Fig. 9c. At the BOA (Fig. 9a) the SW RF has always a cooling effect and varies from  $-93.1$  to  $-0.5 \text{ W m}^{-2}$  while the LW RF has always a heating effect and varies from  $+2.8$  to  $+10.2 \text{ W m}^{-2}$ . The range of values of the SW RF is also consistent with forcing measurements made in southwestern Spain during the summer season (Cachorro et al., 2008) and with Meloni et al. (2003) who found at the island of Lampedusa  $-70.8 \text{ W m}^{-2}$  at the BOA for an AOT of 0.511 at 415 nm. The values of the LW RF are consistent with results obtained by Liao and Seinfeld (1998) among others. At a regional case over West Africa and during an intense dust event, Mallet et al. (2009) found an instantaneous (at noon) SW RF at the BOA similar ( $-86.6 \text{ W m}^{-2}$ ) to case 7 for an AOT of 0.6 at 560 nm and a LW RF larger ( $+15.9 \text{ W m}^{-2}$ ). In the cases with low SW RF (3, 4 and 10) and thus with less impact on the Earth radiative budget, the LW RF is higher than the SW RF (in absolute values). In the other cases the LW RF represents between 11 and 26 % (with opposite sign) of the SW RF, except in case 11 for which the LW contribution is 77 % (with opposite sign). We note that the SW RF of case 11 is the lowest one ( $-12.1 \text{ W m}^{-2}$ ) after the cases 3, 4 and 10.

At the TOA (Fig. 9b) the aerosols have also a cooling effect in the SW spectral range (except for case 7, see explanation below) with a RF ranging from  $-24.6$  to  $-1.3 \text{ W m}^{-2}$ . In the LW spectral range they have a heating effect with a RF ranging from  $+0.6$  to  $+5.8 \text{ W m}^{-2}$ . The LW values are comparable to estimations made from satellite data by Zhang and Christopher (2003). Here again the contribution of the LW RF is high for

## Estimation of mineral dust LW RF

M. Sicard et al.

Title Page

Abstract

Introduction

Conclusions

References

Tables

Figures

◀

▶

◀

▶

Back

Close

Full Screen / Esc

Printer-friendly Version

Interactive Discussion



## Estimation of mineral dust LW RF

M. Sicard et al.

Title Page

Abstract

Introduction

Conclusions

References

Tables

Figures

◀

▶

◀

▶

Back

Close

Full Screen / Esc

Printer-friendly Version

Interactive Discussion



the 3 cases with low SW RF. In the other cases (except case 7) the LW contribution varies between 6 and 26 % (with opposite sign). Case 7, thoroughly documented in Sicard et al. (2012), presents the highest AOT, the lowest single scattering albedo (0.83 at 440 nm) and the highest imaginary part of the refractive index (0.01 at 440 nm). By comparing those results to other studies such as Dubovik et al. (2002) and by looking at CALIPSO (Cloud-Aerosol Lidar and Infrared Pathfinder Satellite Observations) aerosol subtyping observations and MODIS (Moderate Resolution Imaging Spectroradiometer) images, Sicard et al. (2012) concluded that the strong absorbing properties of that case might be due to a mixing of dust with polluted and smoke aerosols. Such a case is remarkable since the strong absorbing properties counteract the usually predominant scattering ones resulting in an unusual positive SW RF at the TOA.

The contribution of the aerosols in the whole atmospheric column is quantified by the atmospheric forcing,  $\Delta F_{\text{ATM}}$ , defined as:

$$\Delta F_{\text{ATM}} = \Delta F_{\text{TOA}} - \Delta F_{\text{BOA}}. \quad (4)$$

The atmospheric forcing is shown in Fig. 9c. If we leave aside all cases for which the SW atmospheric forcings are low, i.e.  $|\Delta F_{\text{ATM}}| < +5 \text{ W m}^{-2}$  (cases 3, 4, 9, 10 and 11), the SW  $\Delta F_{\text{ATM}}$  is positive and ranges from +17.8 to +39.3 (for case 7 it is exceptionally high, +101.5  $\text{W m}^{-2}$ , since the two components at the BOA and at the TOA sum up). For comparison, these values are found to be consistent with those obtained by Mallet et al. (2008) who measured atmospheric forcings slightly higher, +43.1  $\text{W m}^{-2}$ , near the dust source and for higher aerosol loads (AOT of 1.06 at 440 nm). The LW  $\Delta F_{\text{ATM}}$  is negative ranging from  $-4.8$  to  $-2.2 \text{ W m}^{-2}$ , and represents between 4 and 26 % (with opposite sign) of the SW component. Slingo et al. (2006) demonstrated that, in high MD loads ( $1 < \text{AOT} < 4$ ), RTM underestimate slightly the solar absorption within the atmosphere. Assuming that this tendency persists in cases with lower MD loads, SW  $\Delta F_{\text{ATM}}$  might be underestimated and therefore the LW/SW ratio overestimated.

The aerosol heating/cooling rate profiles are shown in Fig. 10. For the sake of clarity all cases are not plotted in the figure. The cases with low SW RF (cases 3, 4 and

10) have been discarded. Among the other cases we have represented the case with the strongest (in absolute value) SW RF (case 11), the one with the lowest SW RF (case 7) and the mean of all cases. The mean SW heating rate profile reaches 0.55–0.57 Kday<sup>-1</sup> between 4 and 6 km, while the mean LW cooling rate profile reaches –0.07 Kday<sup>-1</sup> between 1 and 3 km. For all cases the peak of the SW heating rate profile occurs at a higher altitude than the peak of the LW cooling rate profile. Quantitatively, the mean profile is in good agreement with results from Fouquart et al. (1987), for example, who found daily averaged SW heating rate of 0.7 Kday<sup>-1</sup> and LW cooling rates of 0.2 Kday<sup>-1</sup> for a SW AOT of 0.32. A heating, related to the temperature gradient between the ground and the atmosphere, is visible near the surface for both cases 7 (0.1 Kday<sup>-1</sup>) and 11 (0.12 Kday<sup>-1</sup>). This is not systematic for the other cases.

## 6 Conclusions

This work quantifies the sensitivity of the aerosol direct LW RF including absorption and scattering effects to mineral dust particle microphysical and optical properties, dust plume load (AOT) and height, as well as surface temperature and surface albedo. The sensitivity study was performed with a particle model (fine and coarse mode radius of 0.057 and 0.649 μm, respectively, and AOT of 0.37) representative of the typical long-range transported mineral dust in Barcelona and based on almost eight years of AERONET sun-photometer measurements. It shows that:

- The LW RF has a quasi-linear relationship (with a positive slope) with the AOT both at the BOA and at the TOA.
- The closer the dust plume to the BOA/TOA, the highest the LW RF at the BOA/TOA. A mid-point exists at ~ 3.5 km where the LW RF at the BOA and at the TOA are equals.

## Estimation of mineral dust LW RF

M. Sicard et al.

Title Page

Abstract

Introduction

Conclusions

References

Tables

Figures

◀

▶

◀

▶

Back

Close

Full Screen / Esc

Printer-friendly Version

Interactive Discussion



## Estimation of mineral dust LW RF

M. Sicard et al.

Title Page

Abstract

Introduction

Conclusions

References

Tables

Figures

◀

▶

◀

▶

Back

Close

Full Screen / Esc

Printer-friendly Version

Interactive Discussion



- The LW RF is highly dependent on the coarse mode of the dust size distribution: it becomes significant for radii greater than  $0.1 \mu\text{m}$  and increases strongly up to radii of  $1 \mu\text{m}$ . Between those two radii the dust absorption and the scattering increase.
- The LW RF becomes significant for coarse/fine mode ratio,  $N_c/N_f$ , greater than  $10^{-4}$  and increases strongly up to  $10^{-2}$ . The LW RF produced by MD with a size distribution dominated by small particles represents only 14 % at the BOA and less than 10 % at the TOA compared to that produced by a size distribution dominated by large particles.
- For radii lower than  $0.1 \mu\text{m}$  the scattering properties have no effect on the LW RF. For radii greater than  $0.1 \mu\text{m}$ , the scattering effect contributes to the LW RF up to 18 % at the BOA and up to 38 % at the TOA. The highest contribution is reached for particles with a radius of  $0.5 \mu\text{m}$ .

The shortwave and longwave direct radiative forcing of mineral dust has been estimated in 11 daytime cases over the period 2007–2012 in Barcelona. Measurements from lidar, sun-photometer and satellite were used to constrain the radiative transfer model. We have found that the LW RF varies between  $+2.8$  and  $+10.2 \text{W m}^{-2}$  at the BOA and between  $+0.6$  and  $+5.8 \text{W m}^{-2}$  at the TOA. It represents between 11 and 26 % (with opposite sign) at the BOA and between 6 and 26 % (with opposite sign) at the TOA of the SW component. The LW/SW ratio has no marked tendency with increasing SW RF neither at the BOA, nor at the TOA. The LW atmospheric forcing varies from  $-4.8$  to  $-2.2 \text{W m}^{-2}$ , and the atmospheric LW/SW ratio varies from 4 to 26 % (with opposite sign) and roughly decreases with increasing SW RF. As the LW/SW ratio can reach 26 % at all levels (BOA, TOA and in the atmosphere) it is highly recommended not to neglect the direct LW radiative forcing produced by mineral dust even in daytime studies, unless the authors can explicitly demonstrate that its contribution is small compared to the SW forcing.

The aerosol properties to which the LW RF is sensitive, such as size distribution and concentration, are highly variable with transport. Because of the lack of knowledge of

## Estimation of mineral dust LW RF

M. Sicard et al.

Title Page

Abstract

Introduction

Conclusions

References

Tables

Figures

◀

▶

◀

▶

Back

Close

Full Screen / Esc

Printer-friendly Version

Interactive Discussion



the aerosol properties in the LW range, MD particles remain difficult to accurately parameterize at a large geographical scale in regional and global climate models: the dust load and size distribution as well as the height of the dust plume, on which the LW RF is strongly dependent, are spatially highly variable. In that sense, this study may help to estimate the LW component of the net (shortwave plus longwave) radiative forcing in other Mediterranean regions where the dust load is similar to that of Barcelona.

## Appendix

AERONET size distributions are bimodal volumetric lognormal distributions:

$$\frac{\partial V(r)}{\partial \ln r} = V(r) \frac{\partial N(r)}{\partial \ln r} = \frac{4}{3} \pi r^3 \frac{\partial N(r)}{\partial \ln r}, \quad (1)$$

where  $V$  is the volume,  $r$  the particle radius and  $N$  the particle number. The definitions of the volume median radius,  $r_V$ , and its associated standard deviation,  $\sigma_V$ , can be found at [http://aeronet.gsfc.nasa.gov/new\\_web/Documents/Inversion\\_products\\_V2.pdf](http://aeronet.gsfc.nasa.gov/new_web/Documents/Inversion_products_V2.pdf). The fine and coarse mode separation technique is also explained in the same reference. The median radius of the lognormal distribution (input of the Mie code) relates to  $r_V$  and  $\sigma_V$  as:

$$r_g = r_V e^{-3(\ln \sigma_g)^2}. \quad (2)$$

The standard deviation associated to  $r_g$  is:

$$\sigma_g = \sigma_V. \quad (3)$$

The volume concentration,  $C_V$ , refers to the integration of the volumetric lognormal distribution between minimum and maximum radius:

$$C_V = \int_{r_{\min}}^{r_{\max}} \frac{\partial V(r)}{\partial \ln r} \partial \ln r. \quad (4)$$

From Eqs. (3) and (2) the particle number is derived from:

$$N = \frac{3C_V}{2\pi r_V^3 e^{-\frac{9}{2}\sigma_V} \left[ \operatorname{erf} \left( \frac{\ln r_{\max} - \ln r_V}{\sqrt{2}\sigma} \right) - \operatorname{erf} \left( \frac{\ln r_{\min} - \ln r_V}{\sqrt{2}\sigma} \right) \right]}. \quad (5)$$

*Acknowledgements.* This study was performed in the framework of work package 4 on aerosol-radiation-climate interactions of the coordinated programme ChArMEx (the Chemistry-Aerosol Mediterranean Experiment; <http://charmex.lsce.ipsl.fr>). This work is supported by the 7th Framework Programme project Aerosols, Clouds, and Trace Gases Research Infrastructure Network (ACTRIS) (grant agreement no. 262254); by the Spanish Ministry of Science and Innovation and FEDER funds under the projects TEC2012-34575, TEC2009-09106/TEC, CGL2011-13580-E/CLI and CGL2011-16124-E/CLI. The Earth Sciences Division of the Barcelona Supercomputing Center is acknowledged for the use of the Barcelona AERONET sun-photometer data.

## References

- Basart, S., Pérez, C., Cuevas, E., Baldasano, J. M., and Gobbi, G. P.: Aerosol characterization in Northern Africa, Northeastern Atlantic, Mediterranean Basin and Middle East from direct-sun AERONET observations, *Atmos. Chem. Phys.*, 9, 8265–8282, doi:10.5194/acp-9-8265-2009, 2009.
- Berk, A., Anderson, G. P., Acharya, P. K., Bernstein, L. S., Muratov, L., Lee, J., Fox, M., Adler-Golden, S. M., Chetwynd, J. H., Hoke, M. L., Lockwood, R. B., Gardner, J. A., Cooley, T. W., Borel, C. C., Lewis, P. E., and Shettle, E. P.: MODTRAN5: 2006 Update, in: *Proc. SPIE*, vol. 6233, 62331F, 2006.

## Estimation of mineral dust LW RF

M. Sicard et al.

Title Page

Abstract

Introduction

Conclusions

References

Tables

Figures

◀

▶

◀

▶

Back

Close

Full Screen / Esc

Printer-friendly Version

Interactive Discussion





## Estimation of mineral dust LW RF

M. Sicard et al.

Title Page

Abstract

Introduction

Conclusions

References

Tables

Figures

◀

▶

◀

▶

Back

Close

Full Screen / Esc

Printer-friendly Version

Interactive Discussion



- Cachorro, V. E., Toledano, C., Prats, N., Sorribas, M., Mogo, S., Berjón, A., Torres, B., Rodrigo, R., de la Rosa, J., and De Frutos, A. M.: The strongest desert dust intrusion mixed with smoke over the Iberian Peninsula registered with Sun photometry, *J. Geophys. Res.*, 113, D14S04, doi:10.1029/2007JD009582, 2008.
- 5 Clough, S., Kneizys, F., and Davies, R.: Line shape and the water vapor continuum, *Atmos. Res.*, 23, 229–241, 1989.
- d’Almeida, G., Koepke, P., and Shettle, E.: *Atmospheric Aerosols: Global Climatology and Radiative Characteristics*, A. Deepak Pub, 1991.
- Dubovik, O. and King, M. D.: A flexible inversion algorithm for retrieval of aerosol optical properties from sun and sky radiance measurements, *J. Geophys. Res.*, 105, 20673–20696, 2000.
- 10 Dubovik, O., Smirnov, A., Holben, B. N., King, M. D., Kaufman, Y. J., Eck, T. F., and Slutsker, I.: Accuracy assessment of aerosol optical properties retrieval from AERONET sun and sky radiance measurements, *J. Geophys. Res.*, 105, 9791–9806, 2000.
- Dubovik, O., Holben, B., Eck, T., Smirnov, A., Kaufman, Y., King, M., Tarré, D., and Slutsker, I.: Variability of absorption and optical properties of key aerosol types observed in worldwide locations, *J. Atmos. Sci.*, 59, 590–608, 2002.
- 15 Dubuisson, P., Buriez, J. C., and Fouquart, Y.: High spectral resolution solar radiative transfer in absorbing and scattering media: application to the satellite simulation, *J. Quant. Spectrosc. Ra.*, 55, 103–126, 1996.
- 20 Dubuisson, P., Dessailly, D., Vesperini, M., and Frouin, R.: Water vapor retrieval over ocean using near-infrared radiometry, *J. Geophys. Res.*, 109, D19106, doi:10.1029/2004JD004516, 2004.
- Dubuisson, P., Giraud, V., Chomette, O., Chepfer, H., and Pelon, J.: Fast radiative transfer modeling for infrared imaging radiometry, *J. Quant. Spectrosc. Ra.*, 95, 201–220, 2005.
- 25 Dubuisson, P., Roger, J., Mallet, M., and Dubovik, O.: A code to compute the direct solar radiative forcing: application to anthropogenic aerosols during the Escompte Experiment, in: *Proc. International Radiation Symposium (IRS 2004) on Current Problems in Atmospheric Radiation*, edited by: Fischer, H. and Sohn B.-J., A. Deepak, Hampton, 127–130, 23–28 August 2004, Busan, Korea, 2006.
- 30 Dufresne, J., Gautier, C., and Ricchiuzzi, P.: Longwave scattering effects of mineral aerosols, *American Meteorological Society*, 59, 1959–1966, 2002.
- Forster, P., Ramaswamy, V., Artaxo, P., Berntsen, T., Betts, R., Fahey, D. W., Haywood, J., Lean, J., Lowe, D. C., Myhre, G., Nganga, J., Prinn, R., Raga, G., Schulz, M., and Van Dor-

## Estimation of mineral dust LW RF

M. Sicard et al.

Title Page

Abstract

Introduction

Conclusions

References

Tables

Figures

◀

▶

◀

▶

Back

Close

Full Screen / Esc

Printer-friendly Version

Interactive Discussion



land, R.: Changes in atmospheric constituents and in radiative forcing, in: *Climate Change 2007, The Physical Science Basis, Contribution of Working Group I to the Fourth Assessment Report of the Intergovernmental Panel on Climate Change*, edited by: Solomon, S., Qin, D., Manning, M., Chen, Z., Marquis, M., Averyt, K. B., Tignor, M., and Miller, H. L., Cambridge Univ. Press, Cambridge, UK, 129–234, 2007.

Fouquart, Y., Bonnel, B., Brogniez, G., Buriez, J., Smith, L., Morcrette, J., and Cerf, A.: Observations of Saharan aerosols: results of ECLATS field experiment. Part II: Broadband radiative characteristics of the aerosols and vertical radiative flux divergence, *Journal of Climate Meteorology*, 26, 38–52, 1987.

Gobbi, G. P., Kaufman, Y. J., Koren, I., and Eck, T. F.: Classification of aerosol properties derived from AERONET direct sun data, *Atmos. Chem. Phys.*, 7, 453–458, doi:10.5194/acp-7-453-2007, 2007.

Hess, M., Koepke, P., and Schult, I.: Optical properties of aerosols and clouds: the software package OPAC, *American Meteorological Society*, 79, doi:10.1175/1520-0477(1998)079<0831:OPOAAC>2.0.CO;2, 1998.

Holben, B. N., Eck, T. F., Slutsker, I., Tanre, D., Buis, J. P., Setzer, A., Vermote, E., Reagan, J. A., Kaufman, Y. J., Nakajima, T., Lavenu, F., Jankowiak, I., and Smirnov, A.: AERONET: a federated instrument network and data archive for aerosol characterization, *Remote Sens. Environ.*, 66, 1–16, 1998.

IPCC: *Climate Change 2013: The Physical Science Basis, Contribution of Working Group I to the UN IPCC's Fifth Assessment Report*, Cambridge University Press, New York (USA), 2013.

Kaufman, Y. J., Tanré, D., and Boucher, O.: A satellite view of aerosols in the climate system, *Nature*, 419, 215–223, 2002.

Key, J. and Schweiger, A. J.: Tools for atmospheric radiative transfer: streamer and FluxNet, *Comput. Geosci.*, 24, 443–451, doi:10.1016/S0098-3004(97)00130-1, 1998.

Krekov, G. M.: Models of atmospheric aerosols, in: *Aerosol Effects on Climate*, edited by: Jennings, S. G., University of Arizona Press, Tucson, Ariz., 9–72, 1993.

Lacis, A. and Oinas, V.: A description of the correlated  $k$ -distribution method, *J. Geophys. Res.*, 96, 9027–9064, 1991.

Lau, K. M., Kim, K. M., Sud, Y. C., and Walker, G. K.: A GCM study of the response of the atmospheric water cycle of West Africa and the Atlantic to Saharan dust radiative forcing, *Ann. Geophys.*, 27, 4023–4037, doi:10.5194/angeo-27-4023-2009, 2009.

**Estimation of mineral dust LW RF**

M. Sicard et al.

Title Page

Abstract

Introduction

Conclusions

References

Tables

Figures

◀

▶

◀

▶

Back

Close

Full Screen / Esc

Printer-friendly Version

Interactive Discussion



- Li, J., Ma, X., von Salzen, K., and Dobbie, S.: Parameterization of sea-salt optical properties and physics of the associated radiative forcing, *Atmos. Chem. Phys.*, 8, 4787–4798, doi:10.5194/acp-8-4787-2008, 2008.
- 5 Liao, H. and Seinfeld, J.: Radiative Forcing by mineral dust aerosols: sensitivity to key variables, *J. Geophys. Res.*, 103, 31637–31645, 1998.
- Mallet, M., Pont, V., Lioussé, C., Gomes, L., Pelon, J., Osborne, S., Haywood, J., Roger, J., Dubuisson, P., Mariscal, A., Thouret, V., and Goloub, P.: Aerosol direct radiative forcing over Djougou (northern Benin) during the African Monsoon Multidisciplinary Analysis dry season experiment (Special Observation Period-0), *J. Geophys. Res.*, 113, D00C01, doi:10.1029/2007JD009419, 2008.
- 10 Mallet, M., Tulet, P., Serça, D., Solmon, F., Dubovik, O., Pelon, J., Pont, V., and Thouron, O.: Impact of dust aerosols on the radiative budget, surface heat fluxes, heating rate profiles and convective activity over West Africa during March 2006, *Atmos. Chem. Phys.*, 9, 7143–7160, doi:10.5194/acp-9-7143-2009, 2009.
- 15 Markowicz, K. M., Flatau, P. J., Vogelmann, A. M., Quinn, P. K., and Welton, E. J.: Clear-sky infrared radiative forcing at the surface and the top of the atmosphere, *Q. J. Roy. Meteor. Soc.*, 129, 2927–2947, 2003.
- Mayer, B. and Kylling, A.: Technical note: The libRadtran software package for radiative transfer calculations - description and examples of use, *Atmos. Chem. Phys.*, 5, 1855–1877, doi:10.5194/acp-5-1855-2005, 2005.
- 20 McClatchey, R. A., Fenn, R. W., Shelby, J. E. A., Voltz, F. E., and Garing, J. S.: Optical properties of the atmosphere, Research paper AFCRF-72-0497, Hanscom Air Force Base, Bedford, 108 pp., 1972.
- McConnell, C. L., Formenti, P., Highwood, E. J., and Harrison, M. A. J.: Using aircraft measurements to determine the refractive index of Saharan dust during the DODO Experiments, *Atmos. Chem. Phys.*, 10, 3081–3098, doi:10.5194/acp-10-3081-2010, 2010.
- 25 Meloni, D., di Sarra, A., DeLuisi, J., Di Iorio, T., Fiocco, G., Junkermann, W., and Pace, G.: Tropospheric aerosols in the Mediterranean: 2. Radiative effects through model simulations and measurements, *J. Geophys. Res.*, 108, 4317–4332, 2003.
- 30 Osada, K., Ura, S., Kagawa, M., Mikami, M., Tanaka, T. Y., Matoba, S., Aoki, K., Shinoda, M., Kurosaki, Y., Hayashi, M., Shimizu, A., and Uematsu, M.: Wet and dry deposition of mineral dust particles in Japan: factors related to temporal variation and spatial distribution, *Atmos. Chem. Phys.*, 14, 1107–1121, doi:10.5194/acp-14-1107-2014, 2014.

## Estimation of mineral dust LW RF

M. Sicard et al.

Title Page

Abstract

Introduction

Conclusions

References

Tables

Figures

◀

▶

◀

▶

Back

Close

Full Screen / Esc

Printer-friendly Version

Interactive Discussion



- Otto, S., de Reus, M., Trautmann, T., Thomas, A., Wendisch, M., and Borrmann, S.: Atmospheric radiative effects of an in situ measured Saharan dust plume and the role of large particles, *Atmos. Chem. Phys.*, 7, 4887–4903, doi:10.5194/acp-7-4887-2007, 2007.
- Papayannis, A., Amiridis, V., Mona, L., Tsaknakis, G., Balis, D., Bösenberg, J., Chaikovski, A., De Tomasi, F., Grigorov, I., Mattis, I., Mitev, V., Müller, D., Nickovic, S., Pérez, C., Pietruczuk, A., Pisani, G., Ravetta, F., Rizi, V., Sicard, M., Trickl, T., Wiegner, M., Gerding, M., Mamouri, R. E., D'Amico, G., and Pappalardo, G.: Systematic lidar observations of Saharan dust over Europe in the frame of EARLINET (2000–2002), *J. Geophys. Res.*, 113, D10204, doi:10.1029/2007JD009028, 2008.
- Pey, J., Querol, X., Alastuey, A., Forastiere, F., and Stafoggia, M.: African dust outbreaks over the Mediterranean Basin during 2001–2011: PM<sub>10</sub> concentrations, phenomenology and trends, and its relation with synoptic and mesoscale meteorology, *Atmos. Chem. Phys.*, 13, 1395–1410, doi:10.5194/acp-13-1395-2013, 2013.
- Prospero, J. M., Ginoux, P., Torres, O., Nicholson, S. E., and Gill, T. E.: Environmental characterization of global sources of atmospheric soil dust identified with the Nimbus 7 Total Ozone Mapping Spectrometer (TOMS) absorbing aerosol product, *Rev. Geophys.*, 40, 1002, doi:10.1029/2000RG000095, 2002.
- Remer, L. A., Kleidman, R. G., Levy, R. C., Tanré, D., Mattoo, S., Vanderlei Martins, J., Ichoku, C., Koren, I., Yu, H., and Holben, B. N.: An emerging global aerosol climatology from the MODIS satellite sensors, *J. Geophys. Res.*, 113, D14S07, doi:10.1029/2007JD009661, 2008.
- Ricchiazzi, P., Yang, S., Gautier, C., and Sowle, D.: SBDART: a research and teaching software tool for plane-parallel radiative transfer in the Earth's atmosphere, *B. Am. Meteorol. Soc.*, 79, 2101–2114, doi:10.1175/1520-0477(1998)079<2101:SARATS>2.0.CO;2, 1998.
- Roger, J., Mallet, M., Dubuisson, P., Cachier, H., Vermote, E., Dubovik, O., and Despiou, S.: A synergetic approach for estimating the local direct aerosol forcing: application to an urban zone during the Expérience sur Site pour Contraindre les Modeles de Pollution et de Transport d'Emission (ESCOMPTE) experiment, *J. Geophys. Res.*, 111, D13208, doi:10.1029/2005JD006361, 2006.
- Rothman, L. S., Gordon, I. E., Barbe, A., Benner, D. C., Bernath, P. F., Birk, M., Boudon, V., Brown, L. R., Campargue, A., Champion, J.-P., Chance, K., Coudert, L. H., Dana, V., Devi, V. M., Fally, S., Flaud, J.-M., Gamache, R. R., Goldman, A., Jacquemart, D., Kleiner, I., Lacombe, N., Lafferty, W. J., Mandin, J.-Y., Massie, S. T., Mikhailenko, S. N., Miller, C. E.,

## Estimation of mineral dust LW RF

M. Sicard et al.

Title Page

Abstract

Introduction

Conclusions

References

Tables

Figures

◀

▶

◀

▶

Back

Close

Full Screen / Esc

Printer-friendly Version

Interactive Discussion



Moazzen-Ahmadi, N., Naumenko, O. V., Nikitin, A. V., Orphal, J., Perevalov, V. I., Perrin, A., Predoi-Cross, A., Rinsland, C. P., Rotger, M., Šimečková, M., Smith, M. A. H., Sung, K., Tashkun, S. A., Tennyson, J., Toth, R. A., Vandaele, A. C., and Vander Auwera, J.: The HITRAN 2008 molecular spectroscopic database, *J. Quant. Spectrosc. Ra.*, 110, 533–572, 2009.

Sicard, M., Rocadenbosch, F., Reba, M. N. M., Comerón, A., Tomás, S., García-Vízcaino, D., Batet, O., Barrios, R., Kumar, D., and Baldasano, J. M.: Seasonal variability of aerosol optical properties observed by means of a Raman lidar at an EARLINET site over Northeastern Spain, *Atmos. Chem. Phys.*, 11, 175–190, doi:10.5194/acp-11-175-2011, 2011.

Sicard, M., Mallet, M., García-Vizcaino, D., Comerón, A., Rocadenbosch, F., Dubuisson, P., and Muñoz-Porcar, C.: Intense dust and extremely fresh biomass burning in Barcelona, Spain: characterization of their optical properties and estimation of their radiative forcing, *Environ. Res. Lett.*, 7, 034016, doi:10.1088/1748-9326/7/3/034016, 2012.

Sicard, M., Bertolín, S., Mallet, M., Dubuisson, P., and Comerón, A.: Estimation of a radiative transfer model in the longwave spectral range: sensitivity study and application to real cases, in: *Proc. of the SPIE Remote Sensing*, vol. 8890, doi:10.1117/12.2029471, SPIE, Bellingham, USA, 2013.

Slingo, A., Ackerman, T. P., Allan, R. P., Kassianov, E. I., McFarlane, S. A., Robinson, G. J., Barnard, J. C., Miller, M. A., Harries, J. E., Russell, J. E., and Dewitte, S.: Observations of the impact of a major Saharan dust storm on the atmospheric radiation balance, *Geophys. Res. Lett.*, 33, L24817, doi:10.1029/2006GL027869, 2006.

Sokolik, I. and Golitsyn, G.: Investigation of optical and radiative properties of atmospheric dust aerosols, *Atmos. Environ.*, 27, 2509–2517, 1993.

Sokolik, I., Andronova, A., and Johnson, T. C.: Complex refractive index of atmospheric dust aerosols, *Atmos. Environ.*, 27, 2495–2502, 1993.

Sokolik, I. N., Toon, O. B., and Bergstrom, R. W.: Modeling the radiative characteristics of airborne mineral aerosols at infrared wavelengths, *J. Geophys. Res.*, 103, 8813–8826, 1998.

Stamnes, K., Tsay, S., Wiscombe, W., and Jayaweera, K.: Numerically stable algorithm for discrete-ordinate-method radiative transfer in multiple scattering and emitting layered media, *Appl. Optics*, 27, 2502–2509, 1988.

Tanré, D., Bréon, F. M., Deuzé, J. L., Dubovik, O., Ducos, F., François, P., Goloub, P., Herman, M., Lifermann, A., and Waquet, F.: Remote sensing of aerosols by using polarized,

**Estimation of mineral dust LW RF**

M. Sicard et al.

Title Page

Abstract

Introduction

Conclusions

References

Tables

Figures

◀

▶

◀

▶

Back

Close

Full Screen / Esc

Printer-friendly Version

Interactive Discussion



directional and spectral measurements within the A-Train: the PARASOL mission, *Atmos. Meas. Tech.*, 4, 1383–1395, doi:10.5194/amt-4-1383-2011, 2011.

Vogelmann, A., Flatau, P., Szczodrak, M., Markowicz, K., and Minnett, P.: Observations of large aerosol infrared forcing at the surface, *Geophys. Res. Lett.*, 30, 1655, doi:10.1029/2002GL016829, 2003.

Volz, F.: Infrared refractive index of atmospheric aerosol substances, *Appl. Optics*, 11, 755–759, 1972.

Volz, F.: Infrared optical constant of ammonium sulfate, Sahara dust, volcanic pumice, and flash, *Appl. Optics*, 12, 564–568, 1973.

Volz, F.: Infrared optical constants of aerosols at some locations, *Appl. Optics*, 22, 3690–3700, 1983.

Wagner, F., Bortoli, D., Pereira, S., Costa, M. J., Silva, A. M., Weinzierl, B., Esselborn, M., Petzold, A., Rasp, K., Heinhold, B., and Tegen, I.: Properties of dust aerosol particles transported to Portugal from the Sahara desert, *Tellus B*, 61, 297–306, 2009.

Wang, K., Wan, Z., Wang, P., Sparrow, M., Liu, J., Zhou, X., and Haginoya, S.: Estimation of surface longwave radiation and broadband emissivity using Moderate Resolution Imaging Spectroradiometer (MODIS) land surface temperature/emissivity products, *J. Geophys. Res.*, 110, D11109, doi:10.1029/2004JD005566, 2005.

Yang, P., Feng, Q., Hong, G., Kattawar, G. W., Wiscombe, W. J., Mishchenko, M. I., Dubovik, O., Laszlo, I., and Sokolik, I. N.: Modeling of the scattering and radiative properties of nonspherical dust-like aerosols, *Aerosol Science*, 38, 995–1014, 2007.

Yoshioka, M., Mahowald, N., Conley, A. J., Collins, W. D., Fillmore, D. W., Zender, C. S., and Coleman, D. B.: Impact of desert dust radiative forcing on Sahel precipitation: relative importance of dust compared to sea surface temperature variations, vegetation changes and greenhouse gas warming, *J. Climate*, 16, 1445–1467, doi:10.1175/JCLI4056.1, 2007.

Zhang, J. and Christopher, S. A.: Longwave radiative forcing of Saharan dust aerosols estimated from MODIS, MISR, and CERES observations on Terra, *Geophys. Res. Lett.*, 30, 2188, doi:10.1029/2003GL018479, 2003.

Zhao, C., Liu, X., Ruby Leung, L., and Hagos, S.: Radiative impact of mineral dust on monsoon precipitation variability over West Africa, *Atmos. Chem. Phys.*, 11, 1879–1893, doi:10.5194/acp-11-1879-2011, 2011.

## Estimation of mineral dust LW RF

M. Sicard et al.

Title Page

Abstract

Introduction

Conclusions

References

Tables

Figures

◀

▶

◀

▶

Back

Close

Full Screen / Esc

Printer-friendly Version

Interactive Discussion



**Table 1.** Characteristics of the MD model. Each value in the table is accompanied by a standard deviation.  $r_V$  and  $\sigma_V$  are the volume median radius and standard deviation,  $C_V$  the volume concentration and  $r_g$  and  $N$  the median radius and number concentration.

	Fine mode	Coarse mode
Refractive index	Volz (1983); blue curve in Fig. 1	
$r_V$ [ $\mu\text{m}$ ] ( $r_g$ [ $\mu\text{m}$ ]); $\sigma_V$	$0.146 \pm 0.023$ ( $0.057 \pm 0.013$ ); $0.56 \pm 0.06$	$2.001 \pm 0.297$ ( $0.649 \pm 0.099$ ); $0.61 \pm 0.06$
$C_V$ [ $\mu\text{m}^3 \mu\text{m}^{-2}$ ] ( $N$ [ $\text{cm}^{-3}$ ])	$0.036 \pm 0.018$ ( $13.728 \pm 8.647$ )	$0.176 \pm 0.074$ ( $0.029 \pm 0.010$ )
AOT at 500 nm	$0.37 \pm 0.13$	



## Estimation of mineral dust LW RF

M. Sicard et al.

Title Page

Abstract

Introduction

Conclusions

References

Tables

Figures

◀

▶

◀

▶

Back

Close

Full Screen / Esc

Printer-friendly Version

Interactive Discussion



**Table 2.** Generic parameters for the sensitivity study. The parameters from CERES are accompanied by a standard deviation.

	Value	Source
Atmospheric profiles	Fig. 4 in Sicard et al. (2013)	
Surface albedo	$0.017 \pm 0.001$	CERES spring-summer
Surface temperature	$297.49 \pm 6.56$ K	CERES spring-summer
Aerosol vertical distribution	1.5–3.5 km	Adjusted to model levels after Papayannis et al. (2008)
Zenith angle	$0^\circ$	–

## Estimation of mineral dust LW RF

M. Sicard et al.

**Table 3.** Radiative forcing (last four columns) estimated for the 11 cases for which the MD layer radiative properties have been calculated. Time refers to the lidar start time (all lidar measurements are of a duration of 30 min). AOT is the AOT measured by the sun-photometer at 500 nm.  $\Delta h$  is the overall thickness of the MD layer. S.A. is the surface albedo calculated from the surface emissivity measured by CERES. S.T. is the surface temperature measured by CERES. Mn stands for “Mean”.

Case	Day	Time	AOT	$\Delta h$ [km]	S.A.	S.T. [K]	BOA	TOA	BOA	TOA
							SW	SW	LW	LW
							[W m <sup>-2</sup> ]			
1	21 May 2007	16:11	0.28	4.95	0.017	298.04	-54.8	-15.5	+6.9	+2.1
2	24 May 2007	17:26	0.31	2.76	0.018	298.20	-36.5	-18.6	+6.2	+1.6
3	8 Sep 2008	17:32	0.34	3.60	0.018	300.74	-2.8	-4.0	+5.2	+2.3
4	15 Oct 2008	17:25	0.39	3.75	0.018	297.15	-1.9	-3.4	+4.5	+1.2
5	12 May 2009	17:45	0.38	5.80	0.018	293.80	-53.1	-24.6	+5.9	+1.5
6	21 Jul 2009	18:24	0.38	5.83	0.017	301.15	-55.4	-22.8	+7.4	+5.2
7	22 Jul 2009	12:12	0.59	4.62	0.017	301.49	-93.1	+8.5	+10.2	+5.8
8	12 Apr 2011	09:53	0.17	3.06	0.018	292.29	-24.4	-6.6	+2.8	+0.6
9	22 Aug 2011	18:05	0.24	4.65	0.018	302.63	-16.9	-16.3	+4.3	+2.2
10	1 Sep 2011	18:54	0.23	3.55	0.017	300.68	-0.5	-1.3	+3.7	+1.5
11	28 Jun 2012	18:47	0.50	4.33	0.018	302.05	-12.1	-16.4	+9.3	+4.2
Mn	–	–	0.35	4.26	0.018	298.93	-31.9	-11.0	+6.0	+2.6

Title Page

Abstract Introduction

Conclusions References

Tables Figures

◀ ▶

◀ ▶

Back Close

Full Screen / Esc

Printer-friendly Version

Interactive Discussion



## Estimation of mineral dust LW RF

M. Sicard et al.

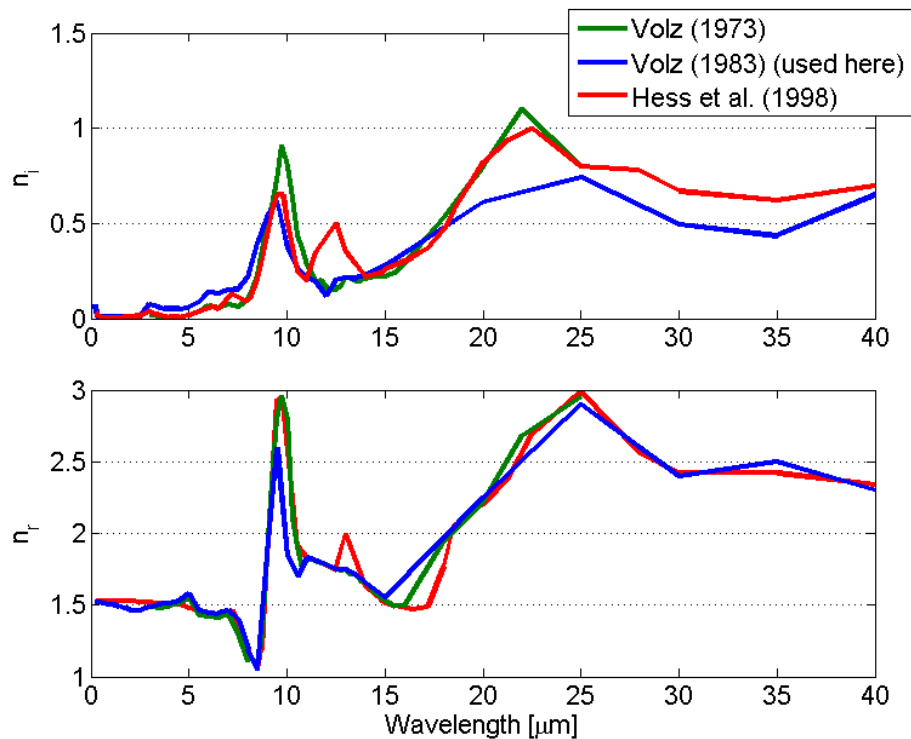


**Fig. 1.** Mineral dust spectral dependency of the (bottom) real part,  $n_r$ , and (top) imaginary part,  $n_i$ , of the refractive index from different literature sources.

[Title Page](#)[Abstract](#)[Introduction](#)[Conclusions](#)[References](#)[Tables](#)[Figures](#)[◀](#)[▶](#)[◀](#)[▶](#)[Back](#)[Close](#)[Full Screen / Esc](#)[Printer-friendly Version](#)[Interactive Discussion](#)

## Estimation of mineral dust LW RF

M. Sicard et al.

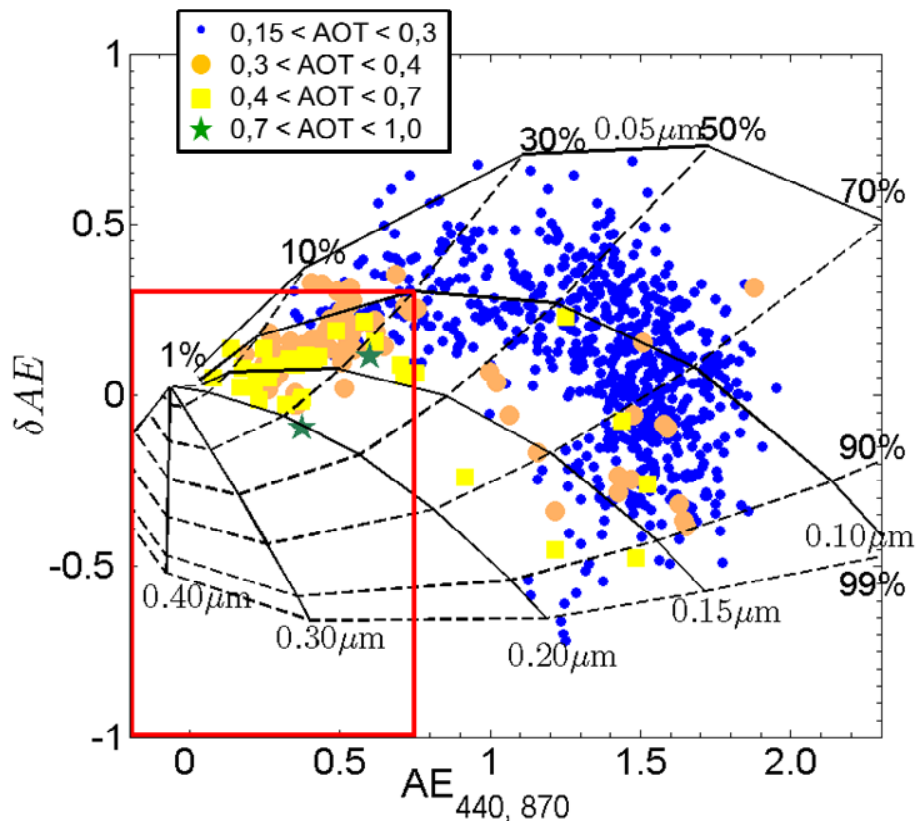


**Fig. 2.**  $\delta AE$  vs.  $AE$  plot diagram for  $n_r = 1.4$  and  $n_i = 0.001$  from AERONET measurements in Barcelona. The black solid lines are each for a fixed fine mode radius,  $r_{g,f}$ , and the dashed black lines for a fixed fraction of the fine mode contribution to the AOT at 675 nm.

Title Page

Abstract

Introduction

Conclusions

References

Tables

Figures

◀

▶

◀

▶

Back

Close

Full Screen / Esc

Printer-friendly Version

Interactive Discussion



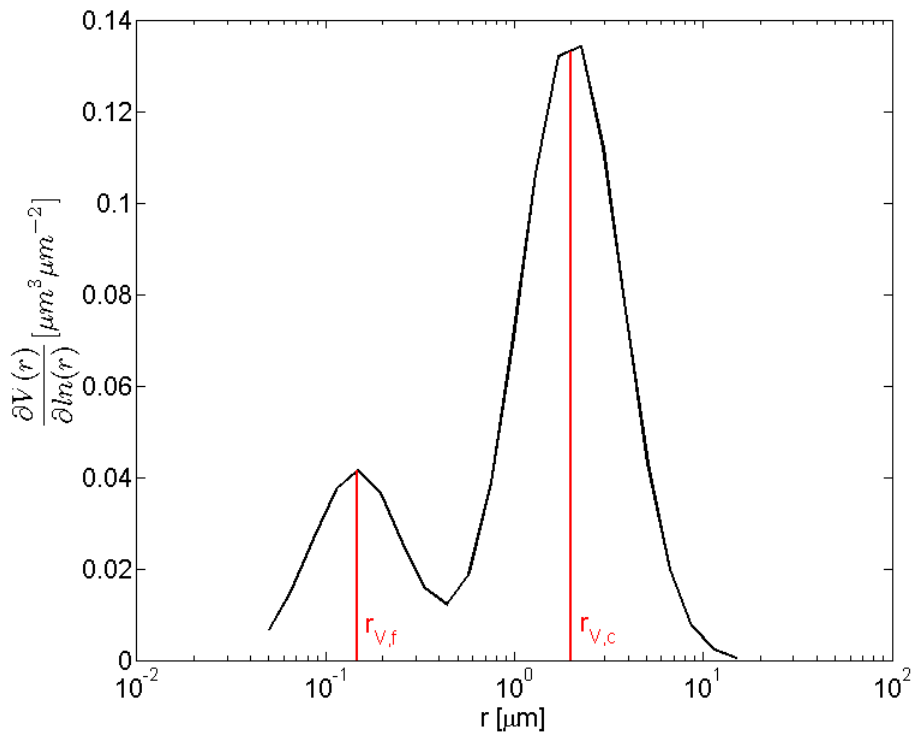


**Fig. 3.** Size distribution of the MD model. It has been calculated as the average of the 134 AERONET size distribution retrievals in Barcelona identified as MD particles in the period 23 December 2004–15 September 2012.

**Estimation of mineral dust LW RF**

M. Sicard et al.

Title Page	
Abstract	Introduction
Conclusions	References
Tables	Figures
◀	▶
◀	▶
Back	Close
Full Screen / Esc	
Printer-friendly Version	
Interactive Discussion	



**Estimation of mineral dust LW RF**

M. Sicard et al.

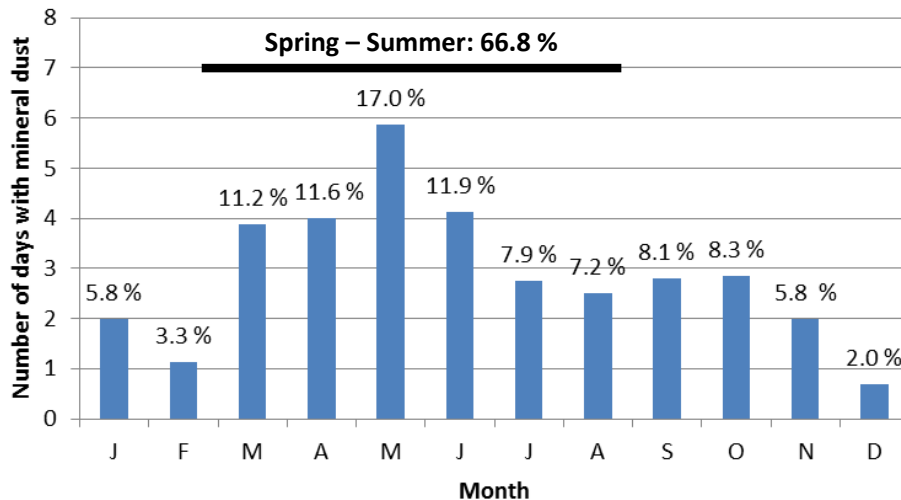


**Fig. 4.** Number of days per month with MD from AEORNET measurements in Barcelona. The numbers above the bars indicate their frequency with respect to the total annual number of days with MD. The number of days with MD in spring and summer represent 66.8 % of the total annual number of days with MD.

[Title Page](#)[Abstract](#)[Introduction](#)[Conclusions](#)[References](#)[Tables](#)[Figures](#)[◀](#)[▶](#)[◀](#)[▶](#)[Back](#)[Close](#)[Full Screen / Esc](#)[Printer-friendly Version](#)[Interactive Discussion](#)

## Estimation of mineral dust LW RF

M. Sicard et al.

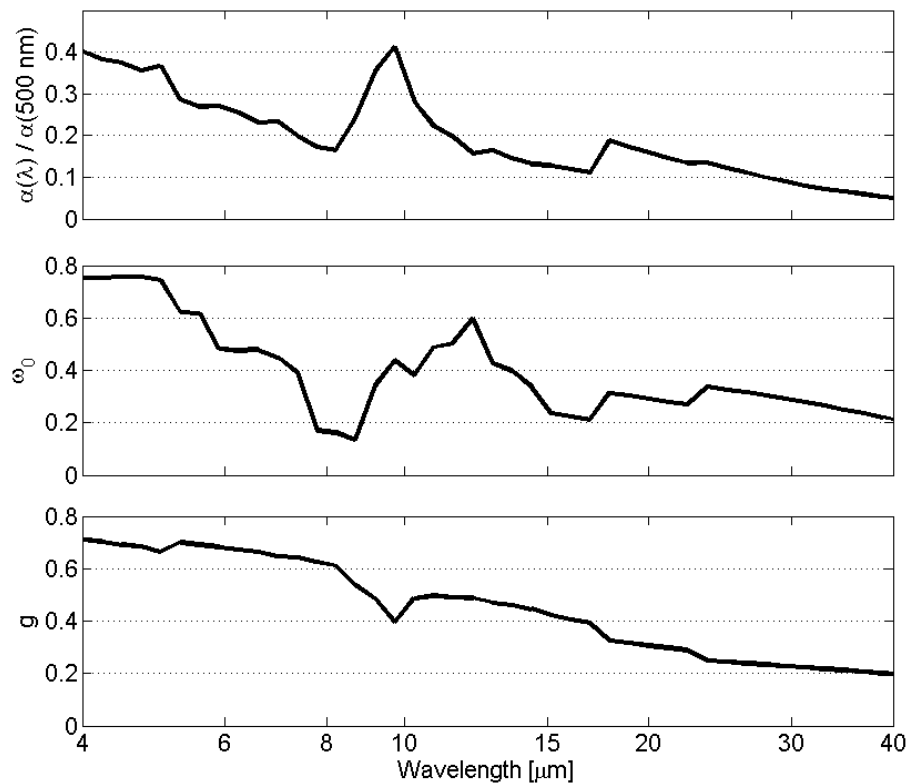


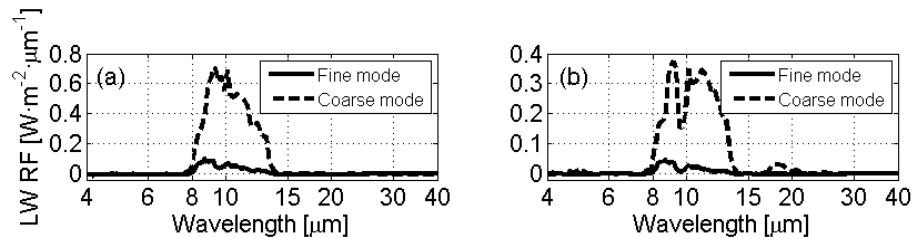
**Fig. 5.** Wavelength-dependency of the optical properties of the bimodal distribution of MD defined in Table 1. (Top) Extinction coefficient normalized at 500 nm, (center) single scattering albedo, and (bottom) asymmetry factor.

[Title Page](#)[Abstract](#)[Introduction](#)[Conclusions](#)[References](#)[Tables](#)[Figures](#)[◀](#)[▶](#)[◀](#)[▶](#)[Back](#)[Close](#)[Full Screen / Esc](#)[Printer-friendly Version](#)[Interactive Discussion](#)



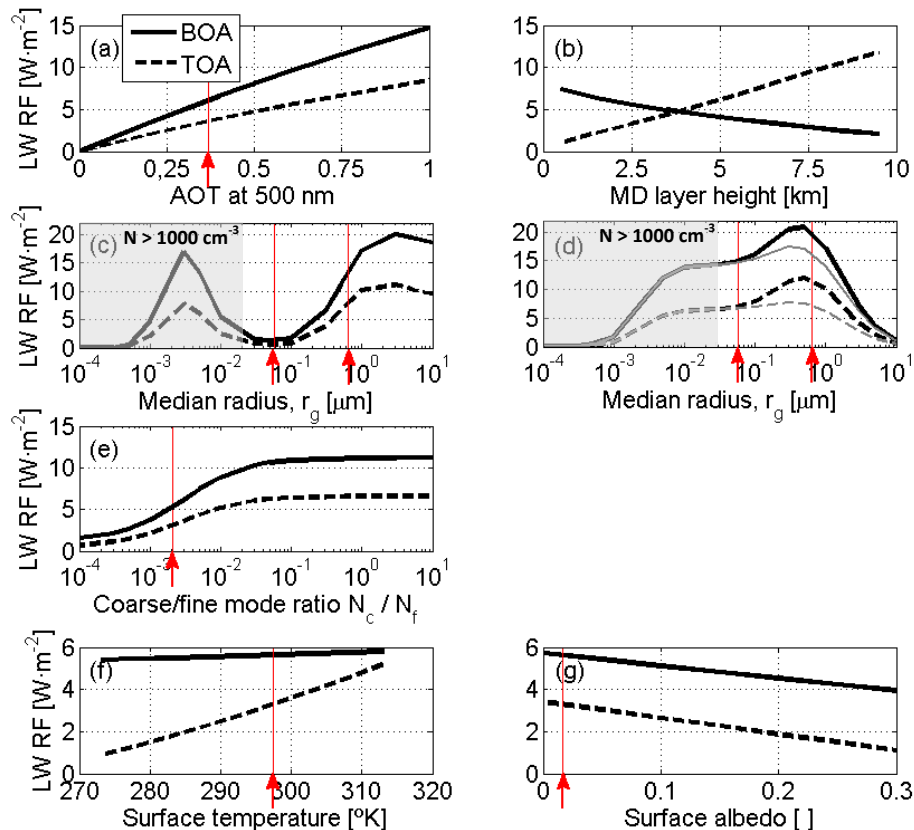
## Estimation of mineral dust LW RF

M. Sicard et al.



**Fig. 6.** Longwave spectral radiative forcing as a function of wavelength at (a) the BOA and (b) the TOA for the fine and coarse mode.

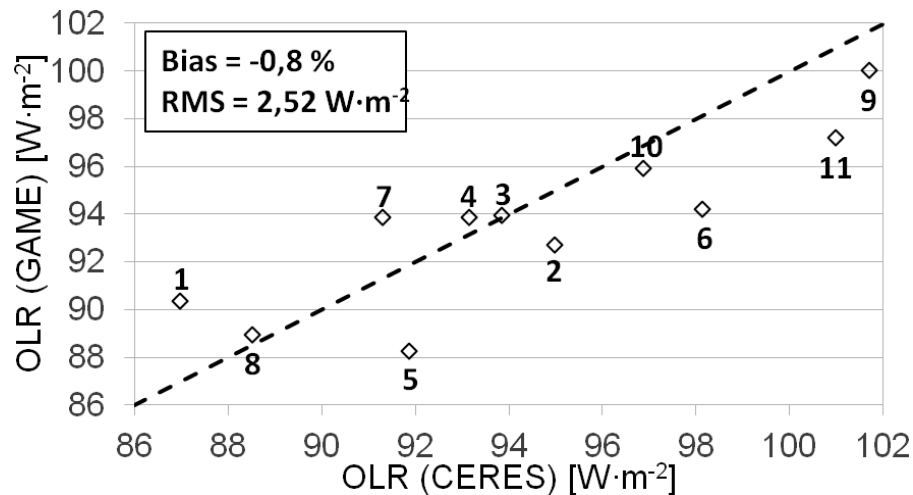
[Title Page](#)
[Abstract](#)
[Introduction](#)
[Conclusions](#)
[References](#)
[Tables](#)
[Figures](#)
[◀](#)
[▶](#)
[◀](#)
[▶](#)
[Back](#)
[Close](#)
[Full Screen / Esc](#)
[Printer-friendly Version](#)
[Interactive Discussion](#)

**Fig. 7.** LW RF as a function of **(a)** AOT at 500 nm, **(b)** MD layer height assuming a 1 km thickness, **(c)** particle median radius maintaining AOT (500 nm) = 0.37 and **(d)** maintaining the volume constant, **(e)** coarse/fine mode ratio  $N_c/N_f$ , **(f)** surface temperature and **(g)** surface albedo. The legend in Fig. 7a is the same for all the plots. In Fig. 7d, the lines in grey represent the RF without considering the aerosol scattering properties. The red arrows indicate the values taken for the MD model.

## Estimation of mineral dust LW RF

M. Sicard et al.



**Fig. 8.** Comparison of the outgoing LW radiation simulated by GAME with that measured by CERES at the TOA. The number below or above each diamond is the case number (see Table 3).

[Title Page](#)[Abstract](#)[Introduction](#)[Conclusions](#)[References](#)[Tables](#)[Figures](#)[◀](#)[▶](#)[◀](#)[▶](#)[Back](#)[Close](#)[Full Screen / Esc](#)[Printer-friendly Version](#)[Interactive Discussion](#)

Estimation of mineral dust LW RF

M. Sicard et al.

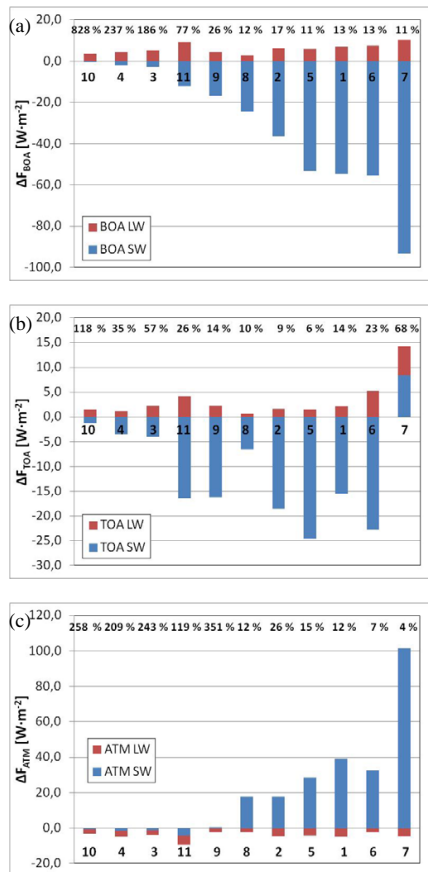


**Fig. 9.** SW and LW RF (a) at the BOA, (b) at the TOA and (c) in the whole atmosphere for the 11 cases. The case number (see Table 3) is indicated below the abscissa axis. The cases are ordered by increasing SW RF (in absolute value) at the BOA. Percentages on top of the graphs represent the LW/SW forcing ratio.

Title Page

Abstract Introduction

Conclusions References

Tables Figures

◀ ▶

◀ ▶

Back Close

Full Screen / Esc

Printer-friendly Version

Interactive Discussion



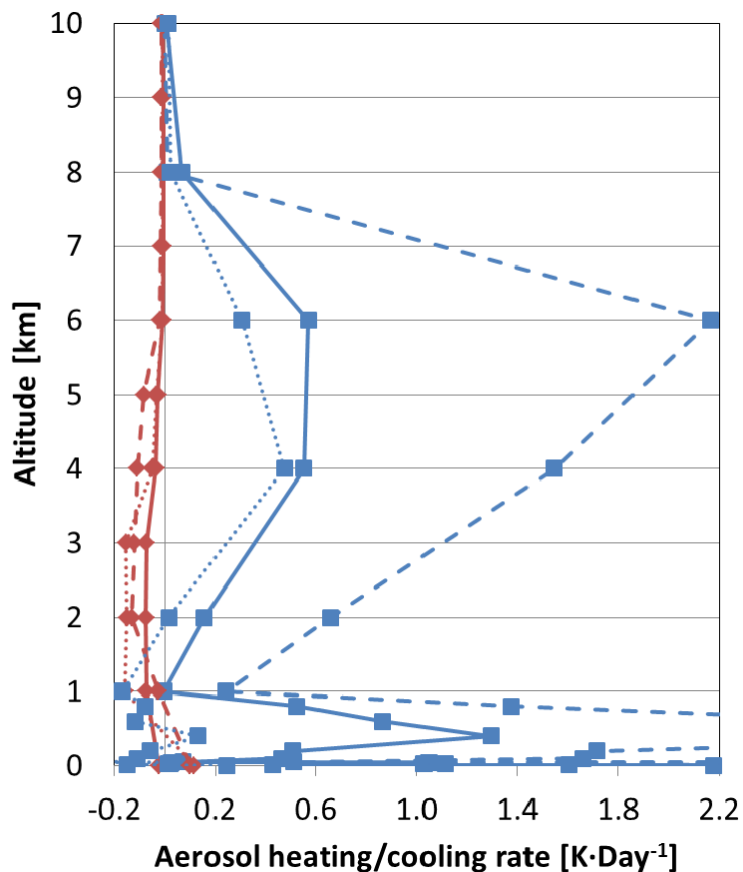


**Fig. 10.** Aerosol heating/cooling rate in the LW (red lines) and in the SW (blue lines) spectral range for case 11 (strongest SW RF at the BOA, dash line). case 7 (lowest SW RF at the BOA, dot line) and the mean of all cases, excepting cases 3, 4 and 10 (solid line).

Estimation of mineral dust LW RF

M. Sicard et al.

Title Page

Abstract Introduction

Conclusions References

Tables Figures

◀ ▶

◀ ▶

Back Close

Full Screen / Esc

Printer-friendly Version

Interactive Discussion

